EFFECT OF LEADING EDGE EROSION ON THE PERFORMANCE OF TRANSONIC COMPRESSOR BLADES

A. Hergt[1], T. Danninger[2], J. Klinner[1], S. Grund[1], M. Beversdorff[1], C. Werner-Spatz[3]

[1] German Aerospace Center (DLR), Institute of Propulsion Technology, Linder Hoehe, 51147 Cologne, Germany, contact: alexander.hergt@dlr.de
[2] ANSYS Germany GmbH, Staudenfeldweg 20, 83624 Otterfing, Germany
[3] Lufthansa Technik AG, Weg beim Jäger 193, 22335 Hamburg, Germany

ABSTRACT

Within this paper an experimental and numerical investigation about the effect of leading edge erosion at transonic blades was performed. The measurements were carried out on a linear blade cascade in the Transonic Cascade Wind Tunnel of DLR in Cologne at two operating points with an inflow Mach number of 1.05 and 1.12. The numerical simulations were performed by ANSYS Germany. The type and specifications of the erosion for the study were derived from real engine blades and applied to the leading edges of the experimental cascade blades using a waterjet process as well as detailed modelled and meshed within the numerical setup. Numerical simulations and extensive wake measurements were carried out on the cascades to evaluate aerodynamic performance. The increase in losses was quantified to be 4 percent as well as a reduction of deflection and pressure rise was detected at both operating points.

KEYWORDS

ERODED LEADING EDGE, TRANSONIC BLADES, PERFORMANCE

NOMENCLATURE

β	flow angle with respect to cascade front	p	pressure
c	profile chord length	Re	Reynolds number based on c
ϵ	cascade deflection angle = β_1-β_2	t	pitch
h	blade span	u,v,w	velocity components
i	incidence angle = $\beta_1 - \beta_{1,Design}$	x,y,z	cartesian coordinates
M	Mach number	ω	total pressure loss coefficient = $\frac{p_{t,1}-p_{t,2}}{p_{t,1}-p_1}$

Subscripts

0	reference state	is	isentropic
1	inlet plane	t	total, stagnation value
2	exit plane		

Abbreviations

ADP	aerodynamic design point	MP2	measurement plane 2 (exit)
AVDR	axial velocity density ratio = $\frac{\rho_2 \cdot v_2 sin\beta_2}{\rho_1 \cdot v_1 sin\beta_1}$	PIV	particle image velocimetry
MP 1	measurement plane 1 (inlet)	ROI	region of interest

INTRODUCTION

Since two decades, fan and compressor blades design for aircraft engines is based on the usage of modern optimization procedures and CFD methods as already shown by Benini (2004) and Voss et al. (2006). At the Beginning, the development led to the use of multi-objective optimizations with the application of Kriging and bayesian trained Neural Network based metamodels as still used for simple aerodynamic profile design as shown by Munoz Lopez et al. (2022). Later on, the importance of including different disciplines was more clearly recognized. This has resulted in the fact, that in today's design processes multiobjective-multidisciplinary optimization procedures.

The resulting highly efficient designed blades are subject to various types of wear and damage as soon as they are in service. And this affects directly the efficiency as well as the fuel consumption of an engine as described in the report of Sallee et al. (1975). They investigated the Pratt & Whitney JT8D engine and could show that 60 to 70 percent of increase in fuel consumption results from a deterioration of the fan and compressor system. In this context, the authors were also faced with the question of how to deal with this knowledge in terms of engine maintenance. Essentially, this means balancing the cost of replacing or repairing fan and compressor blading against increasing fuel consumption and the associated increase in operating costs. However, in order to make a clear statement or decision about what repair efforts are necessary and economic, the mechanisms that are causing deterioration must be identified and their effect must be understood in detail.

In 1995 a first advise concerning the blade refurbishing technique was given by Roberts (1995). Continuing this, Lufthansa Technik AG (LHT), one of the world's largest aircraft engine maintenance companies, started more than ten years ago a long term study to address the questions which are the significant effects, how the deterioration mechanisms are working and what maintenance effort would be economically to achieve efficiency improvement. In the first step, the main damage types were extracted on the basis of engine data from maintenance at LHT as described by Giebmanns et al. (2012). Thereby, the erosion of the leading edge of transonic blading has been shown to be a dominant damage type. This is confirmed by a number of studies during the last decades. Reid and Urasek (1973) showed a significant reduction of efficiency in a single stage compressor caused by an increase of leading edge thickness. Within a further study, Balan and Tabakoff (1984) investigated a low speed compressor cascade and a single stage rig and found a reduction in efficiency which was also based on the changes in leading edge shape. Beside all the investigations on leading edge erosion effects by Roberts et al. (2002), Hamed et al. (2006), Ghenaiet (2012) and Gunn et al. (2022) also the numerical simulation and prediction of this effect becomes important as shown in the study of Tabakoff et al. (1990).

However, within the study of DLR and LHT (Giebmanns et al., 2012) it was apparent that detailed measurements of the effects of leading edge erosion on transonic fans and compressor blades were not available, although they are needed for the description and understanding of the loss mechanisms and for the development of an accurate numerical prediction. Hence, within a detailed pre-study of the influence of a blunt leading edge was investigated by Hergt and Klinner et al. (2014, 2015). Based on this, the current paper deals with the experimental and numerical investigation of a transonic compressor cascade with eroded leading edge, whereby this erosion is derived from real engine blades. The aim of the study is to precisely describe the influence of leading edge erosion on the performance of the cascade in terms of total pressure loss and deflection, and then to identify the mechanisms which are causing it. Thereby and through the

simultaneous validation of the numerical simulations, the basis for the future development of a prediction model and process will be provided.

CASCADE CONFIGURATION

For the study a transonic cascade was used. The blade geometry and cascade parameters are based on a blade section close to 2/3 of blade span (0 means hub and 1 means casing position) of the first high pressure compressor (HPC) rotor of an operating engine. For the experiments the cascade consists of 6 blades with 70 mm chord length and 168 mm blade span was used. Within the numerical simulations only narrow region of 4.5 mm in spanwise direction was meshed as a Q3D setup since the experimental investigations were carried out at blade midspan. The general design parameters of the cascade and the test conditions are shown in Table 1. The measurements and simulations reported are carried out at an inflow Mach number of 1.12 which represents the aerodynamic design point (ADP) and is denotes as OP1 in the paper. In addition, an second operating point OP2 was studied which represents an off-design point of the cascade at inflow Mach number of 1.05. In order to consider the effect of flow contraction within the experimental cascade and make the results comparable with the numerical simulations the axial velocity density ratio (AVDR) was determined. The resulting slightly variation of the AVDR at the different operating points was applied in each case by accordingly deforming the mesh before the simulation. Two different cascade types at both operating points were investigated during the present study. The type A is the reference cascade without any erosion which represents the cascade with new blades. The type B is the

Table 1: CASCADE DESIGN PARAMETERS AND TEST CONDITIONS

Inlet Mach number	M_1	= 1.12 (OP1)	and 1.05 (OP2)		
Inlet flow angle	β_1	= 150.6 deg	Reynolds number	Re	$\approx 1.4\times10^6$
Stagger angle	β_{st}	= 139.9 deg	Flow turning at ADP	$\Delta\beta$	= 9.9 deg
Blade chord length	c	= 70.0 mm	Blade span	h	= 168 mm
Pitch	t	= 49.5 mm	Pitch to chord ratio	t/c	= 0.71

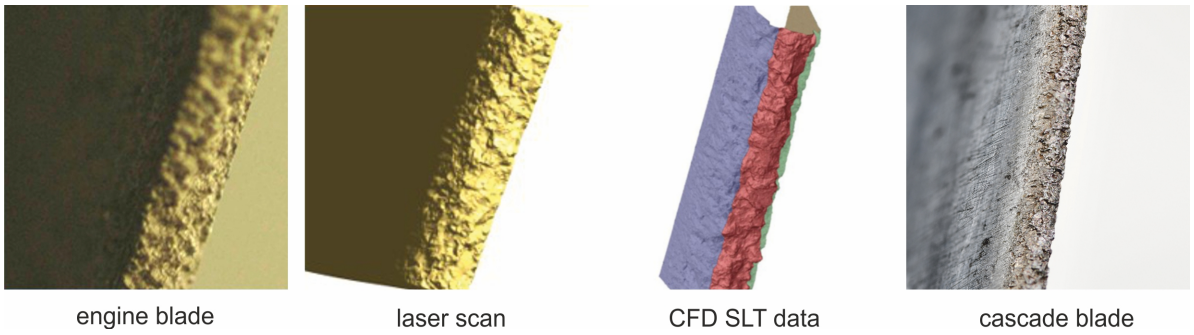

Figure 1: **Comparison of eroded leading edges**

cascade with an eroded leading edge. To enable the most accurate numerical modeling of the experiments, the shape at midspan of the midsection blade was measured of both cascade types. Thereafter, these geometries were used to preparing the CFD setup.

Eroded leading Edge Design

In order to achieve the aim of the study, it is necessary to map the aerodynamic effects resulting from erosion as accurately as possible. Therefore, a laser scan of an eroded leading edge (shown in Fig.1, second from left) of an in-service representative engine blade (shown in Fig.1, left) was performed. Based on the laser scan with four different angles the resulting four SLT data files were combined to the CFD leading edge setup as depicted in Fig.1 (second from right). In order to prepare the experimental setup the characteristics of the eroded leading edge in terms of shape and roughness were also derived from the laser scan. This data were subsequently used to create a comparable leading edge on the blades of the experimental cascade by means of a water jet process which is shown in Fig.1 (right). The blade treatment was carried out by the Frauenhofer Institute of Production Technology.

EXPERIMENTAL SETUP

The experiments were performed in the Transonic Cascade Wind Tunnel (Hergt et al., 2022) at DLR in Cologne. This tunnel is a closed loop, continuously running facility with a variable nozzle, an upper transonic wall in order to reduce shock reflection, and a variable test section height. The air supply system enables an inlet Mach number up to 1.4 and a Mach number independent variation of the Reynolds number from $1x10^5$ to $3x10^6$.

Measurement Technique

Figure 2 shows the cross section of the Transonic Cascade Wind Tunnel test section. Within this figure the position of the inlet measurement plane (MP 1) where the inlet static pressure was measured and the exit measurement plane (MP 2) where the wake measurement with a 3-hole probe was performed are depicted. All results from pressure measurements presented in this study are not time-resolved. Figure 2 also shows the orientation of the PIV light-sheets and the regions of interest (ROI) wich are located at suction and pressure side at the leading edge. A more detailed definition of the measurement planes and cascade parameters is given in Fig. 3.

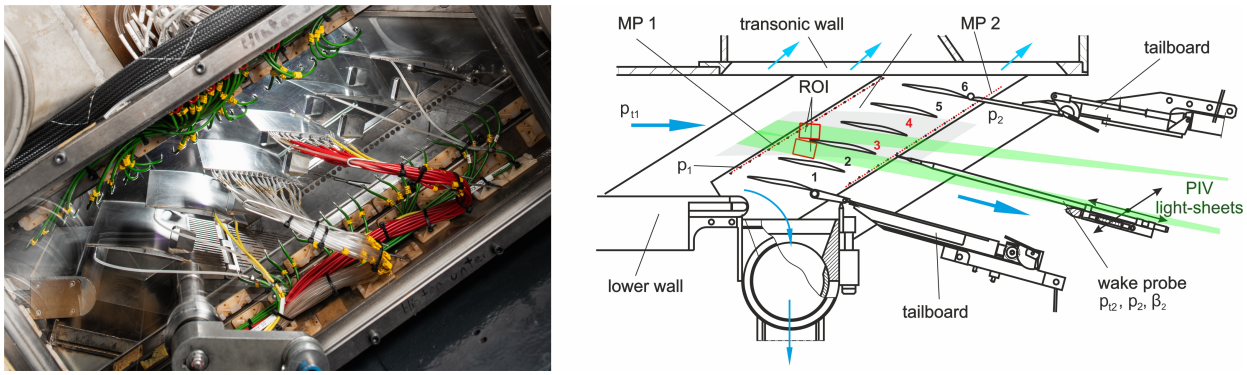

Figure 2: **Figure and cross section of the test section of the DLR Transonic Cascade Wind Tunnel**

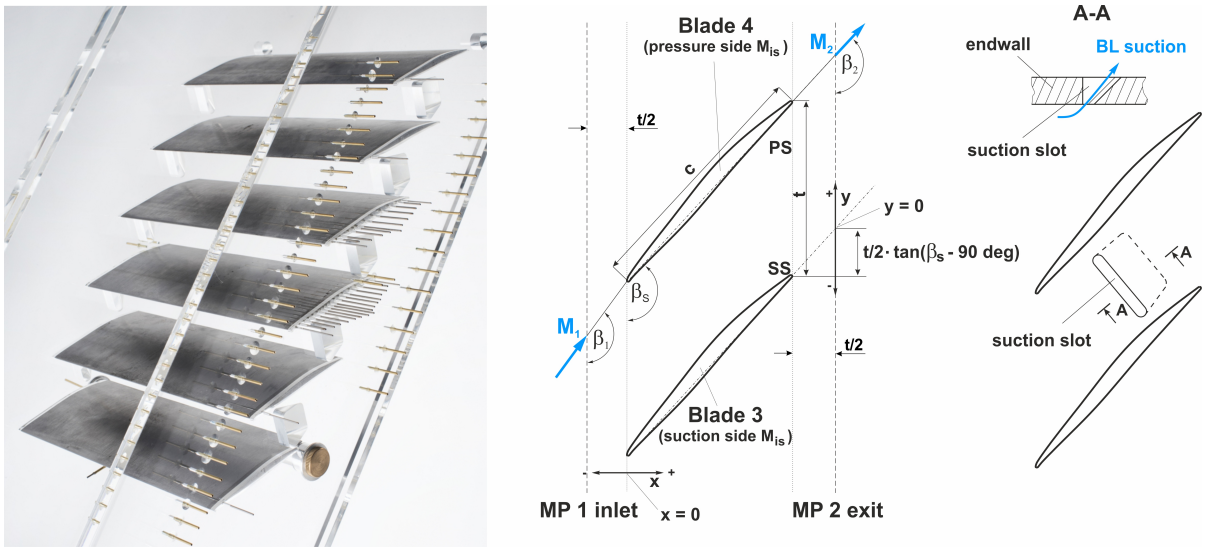

Figure 3: **Transonic compressor cascade, parameters, definition of measurement planes and boundary layer suction design**

Within the experiments laser-2-focus (L2F) measurements (Schodl, 1980) was used to detect the inflow Mach number as well as the inflow angle distribution at cascade midspan at MP 1. In order to ensure comparable operating points during the measurements the boundary layer suction slots depicted in the right hand side of Fig. 3 are necessary to adjust the AVDR Schreiber and Starken [1981]. The isentropic Mach number distribution at the operating points was determined by means of static pressure taps at blade midspan. The estimated uncertainties of the test data at midspan are as follows - mid-span loss coefficient ω: +/- 0.002 - exit flow angle β_2: +/- 0.2 deg - inflow flow angle β_1: +/- 0.2 deg.

NUMERICAL SETUP

The numerical simulations within the present study were carried out with the CFD flow solver Ansys CFX using a stationary approach with a fully coupled solution of Reynolds-averaged conservation equations for mass, momentum, and energy in the flow field (RANS equations). Furthermore, the SST two-equation turbulence model of Menter (1994) with automatic wall treatment was used. This was combined with the Gamma-Theta transition model of Langtry and Menter (2005). The fluid was defined as dry air, treated as single component ideal gas.

In Addition, different boundary conditions are set. All fluid walls of the geometry have a no-split condition and are assumed as hydraulically smooth walls. The walls are assumed to be adiabatic. As only one blade of the cascade is modeled for the CFD simulation, a periodic boundary condition is applied to consider the influence of the neighboring blades. At the sides of the segment, symmetry boundary conditions are applied. The boundary conditions at the inlet of the domain are set according to the measurement values from the experiments and depending on the operating point and the cascade geometry. The following values are applied: Total pressure, total temperature, inflow direction and turbulence level. At the outlet a static pressure is applied, according to the measurement results.

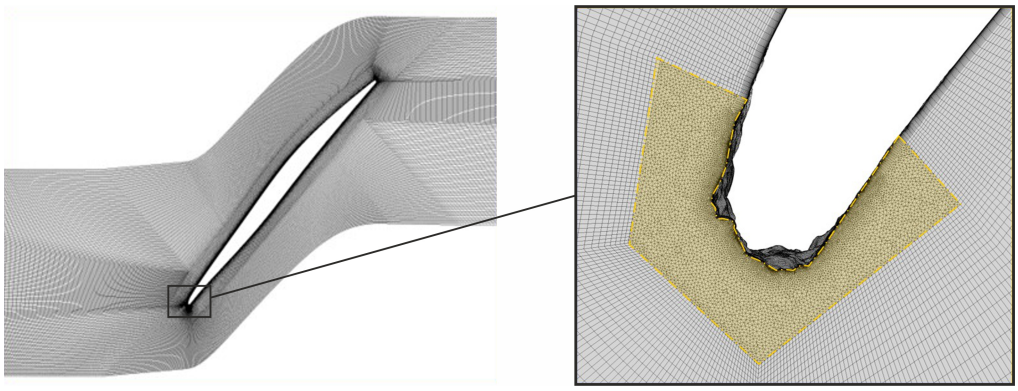

Figure 4: **Hybrid grid with 29 million nodes and 21 prism layers (total height h = 4.5 mm)**

Computational Mesh

Ansys CFX uses a finite-volume method to solve the conservation equations. The conservation equations are integrated over control volumes formed around the corners of the elements, the nodes of the mesh. The flow solution is calculated at these nodes. The mesh was created using the software package Ansys ICEM. The blade region for the reference cascade type A consists entirely of hexahedral elements (3 layers and 1 mm height), whereas for cascade type B a hybrid approach was applied (21 prism layer, 4.5 mm height). This includes an unstructured domain around the leading edge, consisting of tetrahedral elements, to adequately resolve the details of the erosion as depicted in Fig 4. In this area the boundary layer is resolved by prismatic elements. The nodes of the hexahedral part and the unstructured part are conformal and connected, therefore no mesh interface is needed. To avoid interactions of the shock wave with the inlet boundary condition, an increasingly coarse hexdominant mesh is used upstream of the cascade. The Y+ values along the surface are globally kept below 1, with exception of some positions at the leading edge of the eroded blade, where locally higher values appear around the corners of the erosion structures.

RESULTS AND DISCUSSION

In this study, the focus is on the influence of the eroded leading edge on the performance of a compressor blade cascade. In addition, the question of how accurately the cascade flow can be reproduced and predicted by the numerical simulations and what insights into the flow behavior can be obtained from the numerical results will also be answered. The profile Mach number distribution is an essential way to evaluate the performance of a cascade, so the distributions of the two cascade types at both operating points will be reviewed and compared. Figure 5 shows these comparison of experimental and numerical profile Mach number distribution (OP1 left, OP2 right) and first of all it becomes clear that the experimental distributions are well reflected by the numerical results. There are only small differences identifiable between the both cascade types but they reflect essential effects of the flow. In the area of the leading edge along the first 5 percent of the chord length, it can be observed in the numerical results that there is a Mach number peak on the pressure side due to erosion (marked with A). In contrast to this, on the first 5 percent of the suction side the Mach number is slightly decreased thus the small Mach number peak of the reference cascade disappears at erosion cascade.
In general, all suction side distributions show the characteristic behavior of a transonic / super-

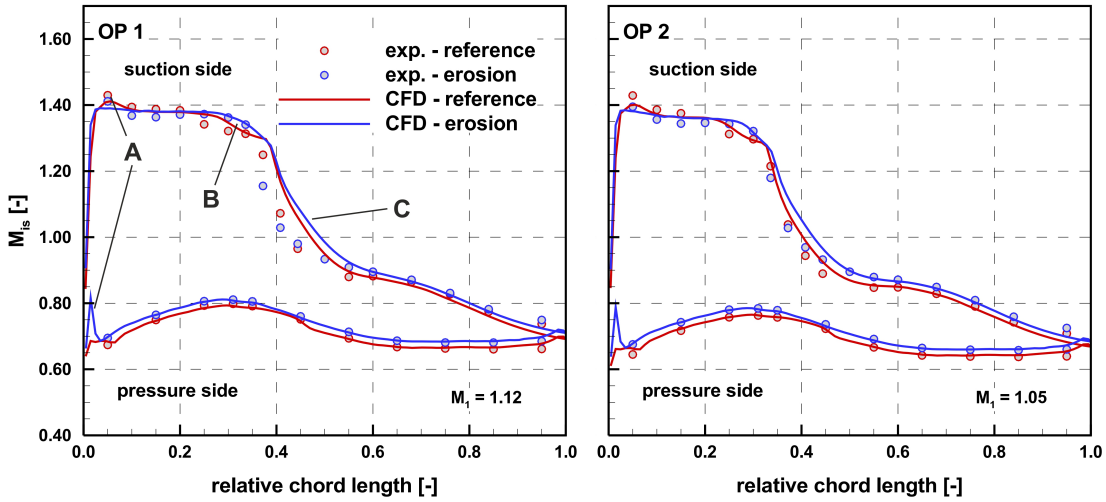

Figure 5: **Experimental and numerical profile Mach number distribution for the reference and erosion cascade at OP1 and OP2**

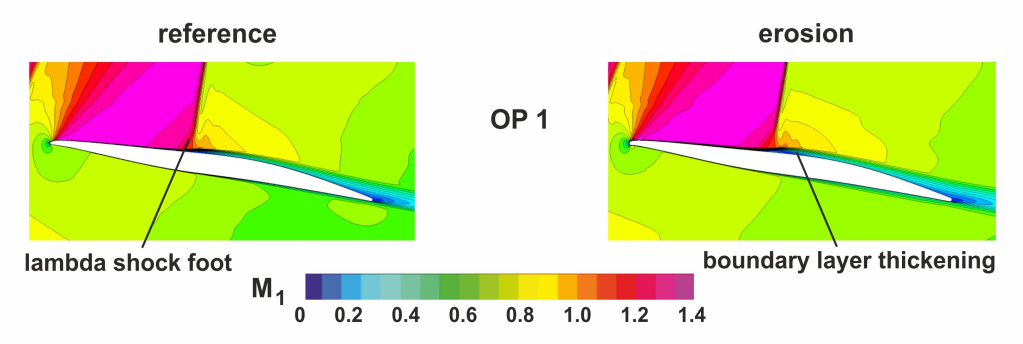

Figure 6: **Numerical blade-to-blade Mach number distribution for the reference and erosion cascade at OP1**

sonic compressor profile which is reflected in the high local Mach number gradient of the plots marked with C. This gradient results from the normal shock within the cascade passage where the flow is decelerated into subsonic. However, at the position marked with C, it is noticeable that there is a discrepancy between the experimental and numerical results. As well, it can be observed that the beginning of the pressure gradient at 38 percent chord length corresponds well for both and that the curves overlap again at 48 percent. The gradient difference can be attributed to a slight change in the structure of the lambda shock above the blade surface. Even small deviations in the numerical and experimental boundary layer can lead to a changed shock boundary layer interaction and thus to a changed shock structure as described by Hergt et al. (2022). Furthermore, this position of the gradient can also be used to determine the averaged position of the shock foot on the blade suction surface. Despite the almost abrupt reduction in Mach number over the shock, the Mach number distribution shows that the deceleration into subsonic on the blade covers about 10 to 15 percent of the chord length. This behavior results

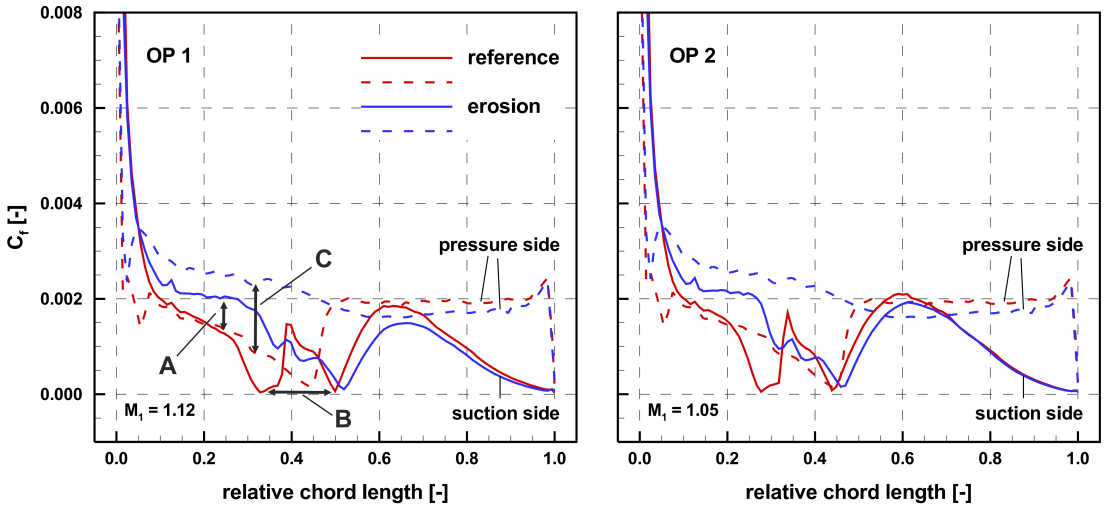

Figure 7: **Numerical wall shear stress coefficient distribution for the reference and erosion cascade at OP1 and OP2**

from the fanning out of the shock into a lambda structure which is caused by the thickening of the boundary layer due to the high pressure gradient as shown in Fig. 6. Moreover, the figure shows that the boundary layer underneath the shock thickens due to the increase in static pressure over the shock. Qualitatively, it can be guessed that there is a difference between the two types of cascades which is probably caused by the affect of the eroded leading edge on the blade boundary layer development. A first indication to clarify this assumption can be found in the Fig. 5. At the point which is marked with B a significant difference in the curve of the Mach number distribution of the two cascade types can be recognized. This indicates that at the reference cascade the suction side boundary layer is laminar up to the shock and in the case with the eroded leading edge, the curve shows a turbulent shock boundary layer interaction. Thus the transition already takes place in front of the shock.
Based on this, it can be noted as a first result that the upstream shifting of the boundary layer transition is a significant effect of the leading edge erosion. But in the next step the question arises how this effect can be quantified. For this purpose, we use the plot of the wall shear stress coefficient C_f on the blade surface in Fig 7. In this figure are three main effects depicted which are marked with A, B and C. First of all, it is noticeable that the value of the wall shear stress coefficient on the suction side beginning from the leading edge up to 30 percent of the blade chord length is significantly lower in the reference case than in the case of the cascade with erosion (marked with A). Furthermore, also on the pressure side the value of the wall shear stress coefficient is much higher on the front 50 percent chord length at the erosion cascade than in the reference case (marked with C). The higher values indicates that the boundary layer transition on the suction and also on the pressure side already takes place in the leading edge region and are caused by the erosion. This is further confirmed by the fact that the laminar separation bubble (marked with B) under the shock on the suction side only appears in the reference cascade.
It should be noted that in the case of the eroded leading edge, the curves shown in Fig. 7 represent averaged results compared to the reference cascade. This results from the fact that the spanwise extent of the numerical simulation is 4.5 mm and the shape of the leading edge is

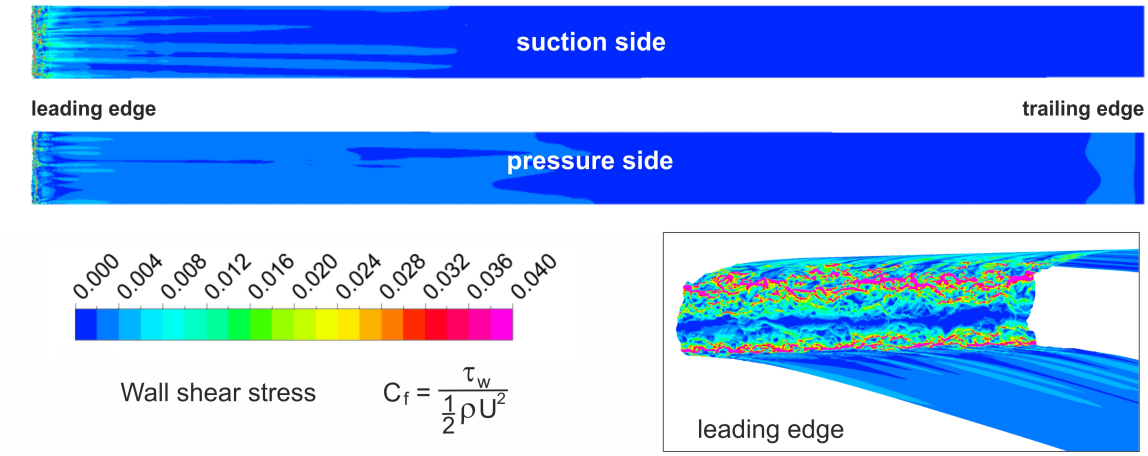

Figure 8: **Numerical wall shear stress coefficient distribution of the eroded leading edge cascade on blade suction and pressure side**

anything but uniform as already described above and depicted in Fig. 8. This figure shows the wall shear stress coefficient distribution on the surface of the cascade blade with leading edge erosion. Here it becomes obvious how non-uniformly the wall shear stress is distributed over the blade height due to the realistic erosion modeling in the simulation. Not taking this effect into account could lead to a significant error in the evaluation.
Based on the higher wall shear stresses caused by the change in the boundary layer behaviour, it is now to be expected that the viscous flow losses are also increased as discussed by Hergt et al. (2021). In order to verify and quantify this assumption, the wakes of the total pressure ratio are shown in Fig. 9. Here, it visible and marked with A that the wake of the erosion cascade is deeper which represents higher viscous losses. The averaged loss coefficient indicates that there is an loss increase of about 4 percent at both operating points.
But this loss increase not only results from the viscous losses caused by the changed boundary layers. In Fig. 9 it is also observable that there is an increase of shock losses within the cascade passage (marked with B). In addition, also a slight shift in the outflow angle distribution is visible at both operating points. This means a slightly reduced deflection of 0.5 deg. at OP1 and of 0.3 deg. at OP2 caused by the erosion, which also results from the change of the boundary layer conditions.
Furthermore, it is to be expected that with higher total pressure losses and a slightly reduced deflection, the static pressure ratio is also influenced. Indeed, the analysis shows that the static pressure ratio has decreased by an average of 2 percent. Thus, the second main result of the study can now be stated, which consists in a significant reduction of the cascade performance in terms of loss and static pressure rise caused by the leading edge erosion. Beside this statement it has to be finally clarified where the higher shock losses come from, what is the causing mechanism behind this behaviour. There two main reasons on which higher shock losses could are causing. One is a higher pre-shock Mach number, which is not detectable in Fig 5. The second reason could be a change within the shock structure in the cascade. Therefor, the shock structure and behaviour is analysed in the case of operating point 1 in more detail.
Figure 10 shows in the upper part the Schlieren pictures and in the lower part the results of

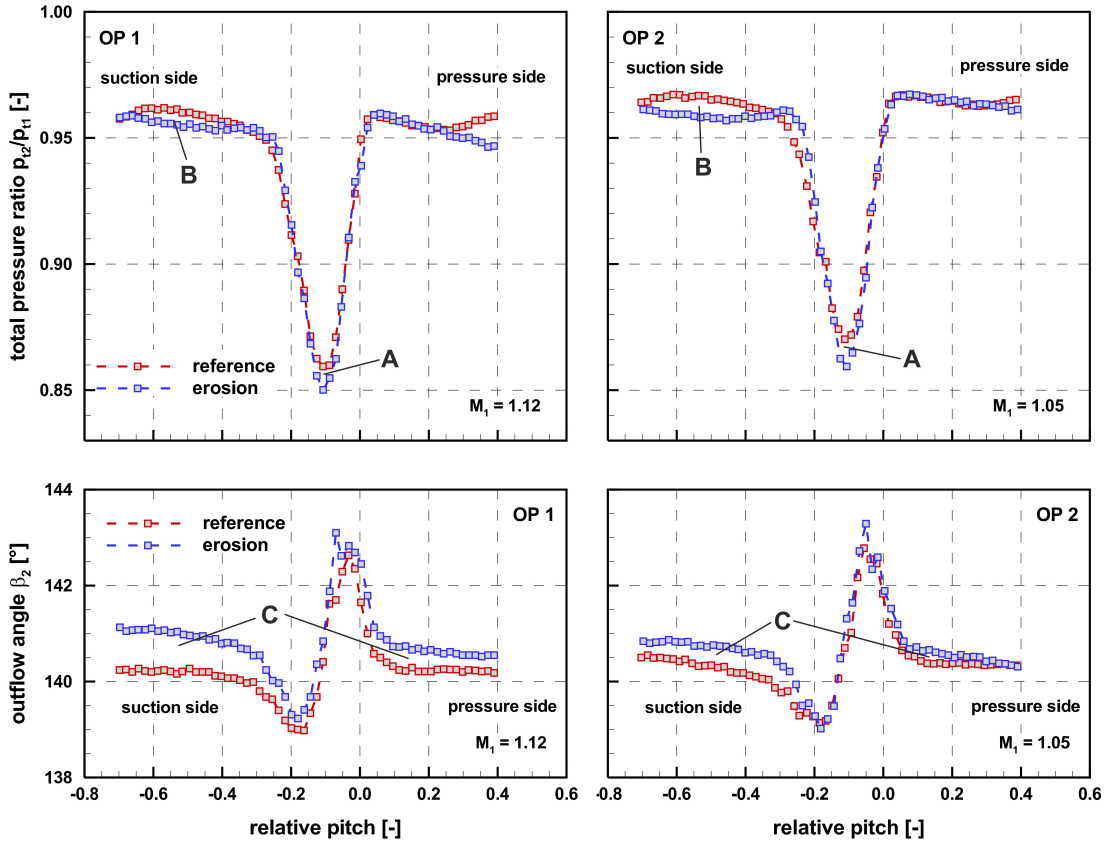

Figure 9: **Profile Mach number distribution for the reference and erosion cascade at OP1 and OP2**

the PIV measurement in the leading edge region of both cascade types. Within this figure it is visible that the curved shape of the bow shock is slightly straightened by erosion as marked with B. Furthermore, the analysis of the PIV results shows an upstream shift of the bow shock of about 10 percent as market with A in the figure. This shift and the more straightened shape of the shock leads to the higher shock losses in the suction side above the blade suction side as marked with B in Fig. 9.

CONCLUSIONS

An experimental and numerical investigation of the effect of an eroded leading edge on the performance of a transonic compressor cascade was performed. For the study, a real eroded leading edge from an operating engine was optically measured and applied to the experimental linear cascade as well as in the numerical setup. The aim was to identify the main effects on the performance of the cascade and there causes.

The first result was to be found that the boundary layer transition is upstream shifted towards the leading edge, which means that no laminar boundary layer is formed on the blade side due to the leading edge roughness. Based on this, the second main result of the study is shown by the reduction of the cascade performance in terms of loss and static pressure rise caused by the erosion. The losses are increased about 4 percent whereas the deflection is reduce by about 0.3

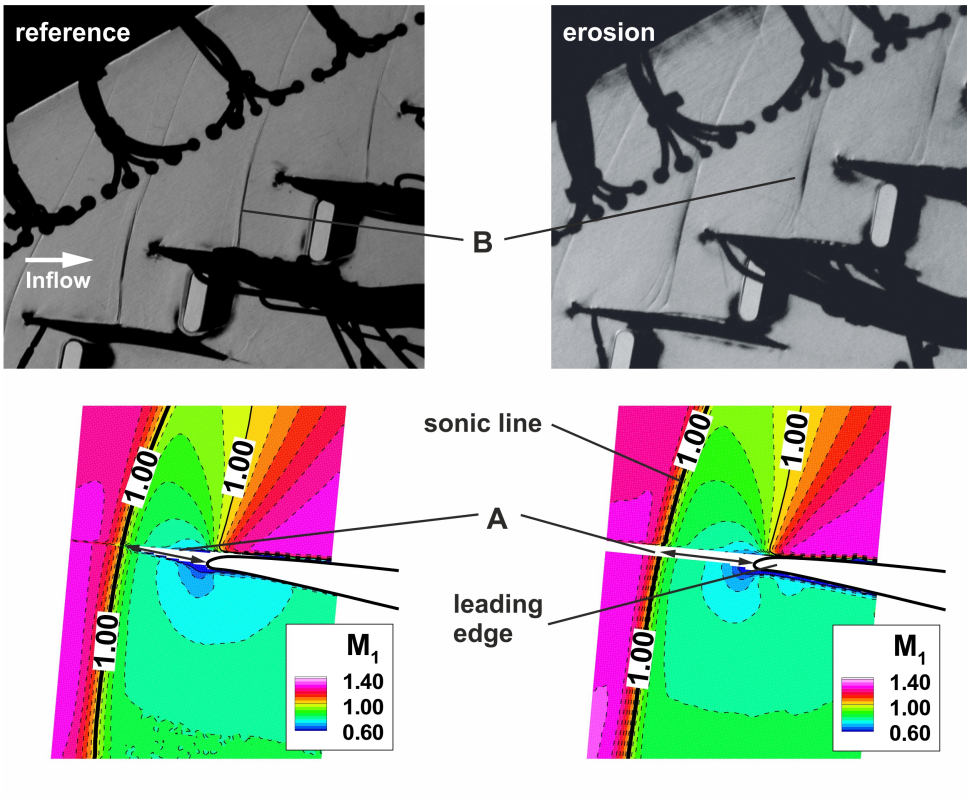

Figure 10: **Experimental Schlieren (top) and PIV measurement results at the leading edge (bottom) for the reference and erosion cascade at OP1**

deg. to 0.5 deg. The operating mechanisms were described in detail as follows. The rise in losses results from an increase in viscous losses due to the changed boundary layer state and from higher shock losses due to a change in the shock structure in front of the leading edge. Furthermore, it was shown that the decrease in deflection results also from the changed boundary layer conditions. Now this knowledge can be used for future prediction of the degradation effects in engine compressor blades.
Finally, it can be stated that the sophisticated modeling of the leading edge erosion within the CFD led to a very good comparability of the numerical and experimental results and the validation of the numerical approach was achieved.

ACKNOWLEDGEMENTS

The investigation reported in this paper was performed under the German Aviation Research Program (LuFo V-3, grant number 20X1706) and is funded by the Federal Ministry of Economics and Technology. The authors would like to thank Lufthansa Technik for the good cooperation within the project.

REFERENCES

C. Balan and W. Tabakoff. Axial Flow Compressor Performance Deterioration. AIAA 20th Joint Propulsion Conference, Cincinnati, OH, USA, November 1984. AIAA.

E. Benini. Three-Dimensional Multi-Objective Design Optimization of a Transonic Compressor Rotor. *Journalof Propulsion and Power*, 20(3):559–565, 2004.

A. Ghenaiet. Study of sand particle trajectories and erosion into the first compression stage of a turbofan. *Journal of Turbomachinery*, 134(5), may 2012. doi: https://doi.org/10.1115/1.4004750.

A. Giebmanns, R. Schnell, W. Steinert, A. Hergt, E. Nicke, and C. Werner-Spatz. Analyzing and Optimizing Geometrically Degraded Transonic Fan Blades by means of 2D and 3D Simulations and Cascade Measurements. Number GT2012-69064 in ASME Turbo Expo, Copenhagen, Denmark, June 11-15 2012.

E. J. Gunn, T. Brandvik, M. J. Wilson, and R. Maxwell. Fan stability with leading edge damage: Blind prediction and validation. *Journal of Turbomachinery*, 144(9), aug 2022. doi: https://doi.org/10.1115/1.4054970.

A. Hamed, W. Tabakoff, and R. Wenglarz. Erosion and Deposition in Turbomachinery. *Journal of Propulsion and Power*, 22(2), March 2006.

A. Hergt, J.Klinner, W. Steinert, S. Grund, M. Beversdorff, A. Giebmanns, and R. Schnell. The Effect of an Eroded Leading Edge on the Aerodynamic Performance of a Transonic Fan Blade Cascade. *ASME Journal of Turbomachinery*, 137:021006–1 – 11, February 2015.

A. Hergt, J. Klinner, S. Grund, C. Willert, W. Steinert, and M. Beversdorff. On the Importance of Transition Control at Transonic Compressor Blades. *ASME Journal of Turbomachinery*, 143(3):031007, March 2021.

A. Hergt, J. Klinner, C. Willert, S. Grund, and W. Steinert. Insights into the unsteady Shock Boundary Layer Interaction. Number GT2022-82720 in ASME Turbo Expo, Rotterdam, The Netherlands, June 2022. ASME.

J. Klinner, A. Hergt, and C. Willert. Experimental Investigation of the transonic flow around the leading edge of an eroded fan airfoil. *Experiments in Fluids*, 55(9):1800, 2014.

R. B. Langtry and F. R. Menter. Transition Modeling for General CFD Applications in Aeronautics. AIAA paper 2005-522. AIAA, 2005.

F. R. Menter. Two-equation eddy-viscosity turbulence models for engineering applications. *AIAA-Journal*, 32(8):1598 – 1605, 1994.

E. J. Munoz Lopez, A. Hergt, and S. Grund. The new Chapter of Transonic Compressor Cascade Design at the DLR. Number GT2022-80189 in ASME Turbo Expo, Rotterdam, The Netherlands, June 2022. ASME.

L. Reid and D. C. Urasek. Experimental Evaluation of the Effects of a Blunt Leading Edge on the Performance of a Transonic Rotor. *Journal of Engineering for Power*, 95(3):199–204, July 1973.

W. B. Roberts. Advanced Turbofan Blade Refurbishment Technique. *ASME Journal of Turbomachinery*, 117, October 1995.

W. B. Roberts, A. Armin, G. Kassaseya, K. L. Suder, S. A. Thorp, and A. J. Strazisar. The effect of variable chord length on transonic axial rotor performance. *Journal of Turbomachinery*, 124(3):351–357, jul 2002. doi: https://doi.org/10.1115/1.1459734.

G. P. Sallee, H. D. Kruckenberg, and E. H. Toomey. Analysis of Turbofan Engine Performance Deterioration and Proposed Follow-On Tests. resreport NASA CR-134769, NASA, 1975.

R. Schodl. A Laser-Two-Focus (L2F) Velocimeter for Automatic Flow Vector Measurements in the Rotating Components of Turbomachines. *ASME Journal of Fluids Engineering*, 102 (4):412–419, December 1980.

H. A. Schreiber and H. Starken. On the Definition of the Axial Velocity Density Ratio in Theoretical and Experimental Cascade Investigation. Symposium on Measuring Techniques in Transonic and Supersonic Flow in Cascades and Turbomachines, Lyon, France, October 15-16 1981.

W. Tabakoff, A. N. Lakshminarasimha, and M. Pasin. Simualtion of Compressor Performance Deterioration Due to Erosion. *ASME Journal of Turbomachinery*, 112, January 1990.

C. Voss, M. Aulich, and B. Kaplan. Automated Multiobjective Optimisation in Axial Compressor Blade Design. Number GT2006-90420 in ASME Turbo Expo, Barcelona, Spain, 08-11 May 2006.

